JCTC Journal of Chemical Theory and Computation

ARTICLE

pubs.acs.org/JCTC

Comparison of Tetrahedral Order, Liquid State Anomalies, and Hydration Behavior of mTIP3P and TIP4P Water Models

Divya Nayar, Manish Agarwal, and Charusita Chakravarty*

Department of Chemistry, Indian Institute of Technology—Delhi, New Delhi 110016, India

ABSTRACT: The relationship between local tetrahedral order, tagged particle potential energy, and coordination number is studied for mTIP3P and TIP4P models of water in the bulk as well as in the neighborhood of a small peptide. The tendency of water molecules with different binding or tagged particle potential energies to occupy environments with different degrees of disorder can be effectively illustrated by constructing tetrahedral order distributions and corresponding entropy metrics conditional on restricted ranges of local binding energy. At the state point corresponding to the onset of the density anomaly, the correlation between tetrahedral entropy versus tagged potential energy is strong and virtually identical for mTIP3P and TIP4P. In TIP4P, this correlation is retained up to temperatures as high as 300 K, while it is lost by 250 K in mTIP3P. In the 250−300 K regime that is important for biomolecular simulations, mTIP3P behaves essentially as a simple liquid while TIP4P shows the density and related anomalies characteristic of water. We also study the number of water molecules, the tetrahedral order, and the tagged molecule potential energies for water molecules as a function of the distance from the peptide for the 16-residue β-hairpin fragment of 2GB1 in mTIP3P and TIP4P solvents. The hydration shell coordination profiles ($n(r)$) of the number of water molecules are almost identical in the two solvents, but the radial variation in the local energies and local order show significant differences. The residue-wise variation in the tagged potential energy of water molecules within the first hydration shell is qualitatively similar in the two models. A comparison of the tetrahedral order distributions of water molecules lying at different distances from the biomolecular solute shows that the perturbation in the local tetrahedral order distributions of the bulk solvent due to the presence of the solute is marginal. Thus, in the 250−300 K regime, the mTIP3P and TIP4P water models show qualitatively different behavior in terms of the relationship between tetrahedral order and local energy, but as solvents in the neighborhood of a biomolecular solute, the differences between the two models are only quantitative and not qualitative.

1. INTRODUCTION

Understanding the relationship between the bulk properties of water and its behavior as a solvent is of central importance in many biomolecular and chemical processes.[1−8] Water has a number of unusual properties that determine its behavior as a solvent. The high dielectric constant of water, associated with strong electrostatic and induction interactions, is responsible for its ability to dissolve polar and charged solutes effectively. The quantum effects associated with the very light hydrogen atoms have a significant effect on the phase diagram, equation of state, and transport properties of water. The fluctuating, three-dimensional, locally tetrahedral liquid state network, held together by hydrogen bonds, gives rise to the thermodynamic and kinetic anomalies of water and plays a crucial role in hydrophobic hydration. An understanding of the complexity of interactions in water, and their consequences for solvation, is necessary in order to understand the relationship between structure, energetics, and dynamics of solvent and solute molecules underlying hydration processes.

Liquids for which the randomly packed, hard-sphere fluid forms a reasonable zeroth-order model are classed as simple liquids.[9] The local coordination in simple liquids is approximately icosahedral with a coordination number between 10 and 12. In contrast, tetrahedral, network-forming liquids have a local coordination of about 4 due to strongly anisotropic, local bonds.[10] Tetrahedrality in water is imposed by the strong, linear hydrogen bonds between oxygen atoms of two neighboring water molecules, with each water molecule forming two donor and two acceptor hydrogen bonds. Increased compression or heating will tend to destroy the tetrahedral bonding and shift the behavior of the system toward that of a simple liquid. Thus a tetrahedral liquid will be dominated by molecules in local environments with tetrahedral symmetry, with a fraction of nontetrahedral local environments that will depend on density and temperature. Tetrahedral liquids can therefore show a density-driven shift in the nature of local orientational order leading to water-like thermodynamic and kinetic anomalies.[11−21] In the case of water, well-known anomalies include the rise in density on isobaric heating (density anomaly) and the increase in molecular mobility on isothermal compression (diffusivity anomaly).[4,7] With decreasing temperature, the energetic bias toward tetrahedral order will tend to increase the fraction of four-coordinate, tetrahedral local environments. In the case of water and silicon, this temperature-dependent change in local tetrahedral order has been predicted to lead to a first-order phase transition between low- and high-density liquids at sufficiently low temperatures. The line of first-order liquid−liquid phase transitions in the pressure−temperature (PT) plane is expected to end in a second critical point.[22−24] In the case of water, low- and high-density amorphous ice forms have been observed, although direct verification of this liquid−liquid critical point (LLCP) is difficult since the associated pressure−temperature regime is difficult to access experimentally. The predicted

Received: April 20, 2011
Published: August 15, 2011

temperature of the LLCP lies between 190 and 232 K, while the predicted pressures range from negative values to as high as 1350 atm.[7,25] An indirect test of the presence of such a second critical point is to look for the Widom line in the experimentally accessible regime, defined as the line of maximum correlation length, or more specifically compressibility maxima, in the PT plane that terminates at the LLCP.[22,23] It should be pointed out that while the thermodynamic and kinetic anomalies of water are well-established experimentally in the supercooled regime, experimental support for the liquid−liquid phase transition and the second critical point remains elusive.

The unusual thermodynamic properties of tetrahedral liquids, as exemplified by water, are expected to affect solvation. Hydration of small hydrophobic solutes, especially the existence of a solubility minimum as a function of temperature along an isobar, has been shown to be strongly sensitive to the equation of state and, therefore, also to the location of the density anomaly in the pressure−temperature (PT) or density−temperature plane.[1,26,27] Given the length-scale dependence of hydrophobicity, with a shift from entropy-driven to enthalpy-driven hydration as solute size increases, the relationship between liquid-state anomalies and hydration behavior may be somewhat different for large hydrophobic solutes.[28−31] Biomolecular solutes, such as proteins and nucleic acids, present an even more complex hydration problem because of their nanoscale size and the presence of polar and nonpolar groups. Interestingly, despite their structural complexity, both categories of biomolecules display an internal dynamical transition for temperatures lying between 180 and 220 K, associated with a sharp rise in the temperature dependence of the mean square atomic displacements (MSDs) of heavy atoms of the biomolecule.[32−36] This dynamical transition has been shown to be largely solvent-driven and conjectured to arise from crossing of the Widom line of compressibility maxima of bulk water.[35] An understanding of the relationship between liquid-state anomalies and hydration behavior would therefore appear to be crucial for designing good interaction potentials for biomolecular simulations. Developing accurate as well as computationally efficient solvent models for water is, however, still a challenge because of the complex interplay of different intermolecular interactions in water like dipole−dipole, dipole−quadrupole, hydrogen-bonding, dispersion, inductive, and repulsive interactions.[37] While *ab initio* approaches for generating water potentials are accurate, they have so far proved cumbersome to implement in bulk simulations .[38,39] The most widely used water models are therefore empirical rigid-body water models which freeze the intramolecular vibrations of the water molecule and model the intermolecular interactions using a distribution of Lennard-Jones and charge-carrying sites on the molecules. These water models were originally developed to reproduce the experimental properties of water under standard conditions. Recent work shows that they differ significantly in their ability to capture features of liquid state anomalies and phase diagrams.[17,18,40−42] For example, the SPC/E model is known to reproduce the anomalous properties of water but at temperatures which are 30−40 K lower than the experimental value of 279 K at 1 atm of pressure.[4,11,43] The version of the TIP3P potential, referred to here as modified TIP3P or mTIP3P, used with the CHARMM force field shows a TMD about 80 K lower than that found experimentally.[41,42,44,45] Four-centered rigid-body water models, especially TIP4P and TIP4P(2005), have been shown to provide the best description of liquid water and ice.[40,46−48] Recent studies by Nutt et al. that compare the effect of three different water models (mTIP3P, TIP4P, and TIP5P) on protein solvation dynamics and structure are of particular interest in this context.[49,50] They found qualitatively similar hydration behavior for all three water models, with relatively small quantitative differences. Interestingly, increasing temperature amplifies the differences between the water models for quantities such as the mean square displacements (MSDs) of heavy atom positions of the solvated protein while attenuating the differences between other quantities, such as reorientational relaxation times.[49]

Since the critical factor controlling the anomalous behavior of water models is the energetic bias toward local tetrahedral order, it is important to understand the relationships between local order and local energy in the presence and absence of solutes. A previous study by Agarwal et al. studied the relationship between local tetrahedral order, local energy, and mobility in bulk water and in the hydration shell of two small peptides, using the CHARMM force field in conjunction with the TIP3P model of water.[51] The local tetrahedral order metric, q_{tet}, associated with an oxygen atom i was defined as

$$q_{tet} = 1 - \frac{3}{8}\sum_{j=1}^{3}\sum_{k=j+1}^{4}\left(\cos\psi_{jk} + \frac{1}{3}\right)^2 \quad (1)$$

where ψ_{jk} is the angle between the bond vectors r_{ij} and r_{ik} where j and k label the four nearest oxygen atoms, so that perfect tetrahedrality corresponds to $q_{tet} = 1$.[11,52] When determining the q_{tet} of water in the neighborhood of a solute, the definition of q_{tet} was extended to include heavy atoms of the peptide like C, O, and N as the nearest neighbors of a water molecule. As a measure of local energy, the tagged molecule potential energy (TPE or u_{tag}), defined as the interaction energy of an individual water molecule with all other molecules in the system, was used.[53−57] The TPE can also be considered as the binding energy of an individual water molecule in the system. In the case of pair-additive potentials, the TPE can be measured as $u_{tag} = U_{tot} - U_{N-1}$ where U_{tot} is total configurational energy of the system consisting of N atoms and U_{N-1} is the configurational energy when a specific molecule is artificially removed from the configuration, keeping the positions of the rest of the atoms unchanged.[58] The Appendix contains the equations for evaluating TPE for a pair-additive intermolecular force field with Lennard-Jones and Coulombic interactions. It should be noted that, for polarizable systems, the definition of the TPE must state whether the environmental polarization is allowed to relax on removal of a given molecule.

The ensemble averages of the measures of local order and local energy were shown to be anticorrelated with each other along isochores of bulk SPC/E and mTIP3P water models.[51] Water in the hydration layer of a peptide showed an oscillatory variation in the TPE with the distance from the peptide for water molecules lying between a 3 and 10 Å radius. These variations were on the order of 2−5% of the bulk TPE value and were anticorrelated with variations in local tetrahedral order in terms of locations of maxima and minima. Within a radius of 3 Å, the perturbation of the solvent structure is very significant, with local TPEs that are 10−15% lower than the bulk value and a fairly strong residue dependence.[51] A recent study of the hydration shell of lysozyme confirms the anticorrelation between the TPE and q_{tet} and shows that both quantities show some sensitivity to different secondary structural units.[59] In this study, we examine the behavior of two common rigid-body water models—mTIP3P and TIP4P—with regard to the relationship between local order and energetics both in the bulk as well as in the hydration shell of a small peptide.

Table 1. Lennard-Jones Parameters (Taken from refs 44 and 45), Dipole Moment (μ), and Quadrupole Moment (Q_T) (Taken from ref 40) for Rigid-Body Water Models TIP3P, mTIP3P, and TIP4P[a]

water models	ε_{OO}	σ_{OO}	ε_{HH}	σ_{HH}	q_O	q_H	q_M	μ	Q_T	μ/Q_T
TIP3P	0.152	3.151			−0.834	0.417		2.35	1.721	1.363
mTIP3P	0.152	3.151	0.046	0.400	−0.834	0.417		2.35	1.721	1.363
TIP4P	0.155	3.150				0.520	−1.04	2.18	2.147	1.014

[a] The units for energy, length, charge, dipole moment, quadrupole moment, and ratio μ/Q_T are kcal mol^{-1}, Å, e, Debye, Debye·Å, and Å^{-1}, respectively.

Table 2. Average Pressure Values for NVT Bulk Water Simulations of mTIP3P and TIP4P Using NAMD

water model	ρ (g cm^{-3})	T (K)	$\langle P \rangle$ (katm)	error$_P$ (katm)
mTIP3P	1.00	260	−0.718	0.0036
	0.95	202	−1.674	0.0031
TIP4P	1.00	260	0.074	0.0036
	0.98	257	−0.007	0.0011

These two water models have essentially the same rigid-body geometry and Lennard-Jones parameters for the oxygen−oxygen repulsion−dispersion interaction (see Table 1). The additional Lennard-Jones sites on the hydrogen atoms are relatively inconsequential for determining bulk structure and dynamics.[60] The critical difference between the two models is the location of the charged sites, which implies very different electrostatic interactions. In the case of mTIP3P and TIP4P, for example, this results in very different quadrupole moments even though dipole moments are similar.[61,62] Since the two water models have very different temperature regimes for the anomalies, the differences in hydration behavior in the two solvent models should allow one to assess the impact of liquid-state anomalies on hydration behavior. We perform a detailed analysis of tetrahedral order distributions, local energy distributions, and coordination number for mTIP3P and TIP4P to establish the nature of correlation between these three parameters which characterize the local environment of water molecules. Though it is intuitively obvious that the tetrahedral order, local energy, and coordination number of water are related, the quantitative correlations have not been examined in great detail, and previous studies have largely focused on the ensemble-averaged values of the two quantities.[51] We also perform simulations of the 16-residue β-hairpin fragment of the 2GB1 protein in both mTIP3P and TIP4P solvents. We examine the order and energetics of mTIP3P and TIP4P solvent molecules as a function of the distance from the peptide. The energetics within the hydration shell are examined by computing the TPEs in the neighborhood of different amino acid residues. We relate the differences in hydration shell structure and energetics between the two solvent models to the differences in the parametrization of the water models. Computational details of the simulations are given in section 2. Results are contained in section 3, and our conclusions are presented in section 4.

2. COMPUTATIONAL DETAILS

2.1. Bulk Water. The bulk water simulations consisted of a system of 256 molecules of TIP3P, mTIP3P, or TIP4P in cubic simulation cells. These rigid-body potential energy surfaces for water are described by contributions from short-range interactions defined by Lennard-Jones potential and long-range electrostatic interactions which were calculated using Ewald sums. The parametric form of the interaction between two water molecules a and b is given by:

$$U_{ab} = \sum_i \sum_j \frac{q_i q_j}{r_{ij}} + 4\epsilon \left(\frac{\sigma^{12}}{r_{OO}^{12}} - \frac{\sigma^{6}}{r_{OO}^{6}} \right) \quad (2)$$

where i and j index partial charges located on molecules a and b respectively and r_{OO} refers to the distance between the oxygen atoms of the two monomers. The potential energy parameters used for TIP3P, mTIP3P, and TIP4P are given in Table 1.

For studying bulk water, we used the DL_POLY molecular dynamics package[63,35] as well as the NAMD biomolecular suite.[66,67] The DL_POLY package was used to ensure consistency with our previous work on water, in particular, the evaluation of the tagged molecule potential energies discussed in the Appendix.[42,51] The NAMD package is more convenient for biomolecular simulations, and as a check on the TPE evaluation procedure using the *pairInteraction* command, we ran bulk water simulations with NAMD 2.7. All bulk water simulations were carried out in a canonical (NVT) ensemble with a time step of 1 fs, and production runs were carried out for 4 ns. The equations of motion were integrated using the Verlet leapfrog algorithm in DL_POLY simulations and velocity Verlet algorithm in NAMD simulations. The rigid-body constraints were implemented using the SHAKE algorithm in DL_POLY simulations and RATTLE algorithm in NAMD simulations. The calculation of long-range electrostatic contributions to configurational energy is done by using different methods in DL_POLY and NAMD. DL_POLY uses Ewald sums, whereas NAMD uses the particle mesh Ewald (PME) method (see Appendix A for details). The results of TPE for bulk system were found to be identical for both the cases.

Simulations of the TIP3P system were carried out for temperatures ranging from 170 K to 300 K and densities ranging from 0.90 g cm^{-3} to 1.20 g cm^{-3}. Simulations for TIP4P and mTIP3P water were carried out at 1.00 g cm^{-3} density and at temperatures ranging from 200 K to 350 K. The state point of (260 K, 1.00 g cm^{-3}) has been examined in detail for mTIP3P and TIP4P. For all of the state points, the compressibility was positive and the system was homogeneous, even at negative pressures, indicative of thermodynamic stability. Table 2 tabulates NVT ensemble results respectively for selected state points of bulk water. The oxygen−oxygen radial distribution functions of mTIP3P and TIP4P at 300 K and 1.00 g cm^{-3} were shown to reproduce those available in the literature.[68] Error bars on the structural and TPE distributions were found to be less than the symbol size in the associated figures.

2.2. Solvated Peptide. The solvated system of peptide was prepared by extracting the 16-residue C-terminal fragment of immunoglobulin binding domain of streptococcal protein G (PDB ID: 2GB1) and then solvating this β-hairpin fragment with 1774 TIP4P water molecules.[51,69] The C-terminal and N-terminal residues did not carry any charges. The two aspartic acids and two glutamic acids had negative charges on their side chains, and one lysine residue carried positive charge. Thus, the solvated peptide had a net −3 charge. In order to maintain charge neutrality, three waters were replaced by three sodium ions in the system. The solvation and ionization were done in a cubic box using the "*solvate*" and "*autoionize*" plugins of VMD 1.8.7, respectively.[70,71]

Table 3. Length of Cubic Simulation Cells and Density (ρ) of Water in System of Peptide Solvated with mTIP3P and TIP4P at 250 K and 300 K

	boxlength (Å)		ρ (g cm^{-3})	
temperature (K)	TIP4P	mTIP3P	TIP4P	mTIP3P
250	37.89	37.09	0.973	1.020
300	38.32	37.67	0.950	0.972

Molecular dynamics simulations of the solvated peptide system were done with both mTIP3P and TIP4P using the NAMD 2.7 package. The CHARMM22 force field was used for the simulations. To compute the short-range interactions, a cutoff equal to half the box length was used. The contribution of long-range electrostatic interaction to the configurational energy was computed using the particle mesh Ewald (PME) method. Energy minimization was done using the conjugate gradient method to remove any steric repulsions among molecules of the system which may arise during the system preparation. The energy minimized system was then subjected to heating in an isobaric−isothermal (NPT) ensemble, at the rate of 1 K per 2500 steps until 250 K was reached and then 1 K per 7500 steps from 250 K to 300 K at 1 atm of pressure. The system was then equilibrated in the NPT ensemble in order to obtain the equilibrated volume value. The resulting box lengths of the cubic box of solvated peptide at 300 K and 250 K are given in Table 3. Using this equilibrated value of volume, the production runs were carried out in the microcanonical (NVE) ensemble for 2 ns using a time step of 2 fs. The configurations were stored every 100 steps (0.2 ps). The keyword *pairInteraction* was used to calculate the tagged potential energy of a given water molecule with all other molecules in the solvated peptide system. Note that the time step is consistent with that used in previous studies.[69] Tables 4 and 5 show the NVE simulation results for pressure and temperature with associated checks on the error; the drift in temperature and pressure is not significant during the course of the run. Error bars on the structural and TPE distributions were found to be less than the symbol size in the associated figures.

3. RESULTS AND DISCUSSION

3.1. Tetrahedral Order and Energetics in Bulk Water. *3.1.1. Distributions of Tetrahedral Order, Tagged Potential Energy, and Coordination Number.* The liquid-state anomaly that is expected to affect solvation thermodynamics is the density anomaly, corresponding to a temperature-density regime for which $(\partial\rho/\partial T)_P > 0$. The boundary of this regime of anomalous density behavior is defined by state points for which $(\partial\rho/\partial T)_P = 0$, i.e., the locus of extrema of the $\rho(T)$ curve along isobars. In the case of water, the temperatures of minimum density occur in a thermodynamically unstable regime, and therefore only the locus of temperatures of maximum density (TMD) can be defined. The state point corresponding to the maximum temperature along the TMD locus in the $\rho-T$ plane corresponds to the temperature of onset of thermodynamic anomalies and is denoted by $(T^{max}_{TMD},\rho^{max}_{TMD})$. The onset temperature for thermodynamic anomalies of various rigid-body water models has recently been determined. The $(T^{max}_{TMD},\rho^{max}_{TMD})$ state points for mTIP3P and TIP4P correspond to (202 K, 0.95 g cm^{-3}) and (257 K, 0.98 g cm^{-3}), respectively.[42] The corresponding state point for the original TIP3P model is (205 K, 0.96 g cm^{-3}).

Table 4. Average Pressure and Average Temperature Obtained from NVE Simulations for Solvated System of Peptide with mTIP3P and TIP4P

water model	target temperature (K)	$\langle T\rangle$ (K)	$\langle P\rangle$ (katm)	error$_T$ (K)	error$_P$ (katm)
mTIP3P	300	301.56	0.092	0.0102	0.0010
	250	252.09	0.249	0.0276	0.0033
TIP4P	300	305.05	−0.141	0.0345	0.0032
	250	253.09	0.097	0.0287	0.0031

Tetrahedral order distributions for water models in the anomalous regime are known to have a very prominent shoulder structure indicative of comparable fractions of tetrahedral and nontetrahedral local environments. In this structurally anomalous regime, tetrahedral order (q_{tet}) is strongly correlated with translational order (τ), which measures the extent of pair correlation between oxygen atoms.[11] The structurally anomalous regimes of all of the rigid-body water models are essentially superimposable in the $q_{tet}-\tau$ plane, even though the temperature and density regimes for the anomalies may be very different.[42] An interesting illustration of this is shown in Figure 1a where the $P(q_{tet})$'s of mTIP3P, TIP4P, SPC/E, and TIP3P at their respective T^{max}_{TMD} values are shown to be essentially superimposable. This was earlier shown to be true for the temperature of maximum density along the 1 atm isobar for some water models but not placed in the context of the similarity in the order maps.[72,73] In the case of the two specific models of interest in this study (mTIP3P and TIP4P), the q_{tet} distributions of the two water models are very different at a given temperature; as illustrated in Figure 1b at (260K, 1.00 g cm^{-3}). The peak at 0.8−0.9 corresponding to strongly tetrahedral local environments is significantly diminished for the mTIP3P model indicating that mTIP3P behaves essentially as a simple liquid while TIP4P is an anomalous, tetrahedral liquid at 260 K.

To contrast the structural information contained in the tetrahedral order distributions with that in the radial distribution function, Figure 2b compares the oxygen−oxygen RDFs of TIP4P and mTIP3P at (260 K, 1.00 g cm^{-3}). While the reduced structuring of the mTIP3P RDF compared to that of TIP4P is obvious, the nature of change in local order is much more evident from the $P(q_{tet})$ distributions in Figure 1b. Figure 2a shows that the RDFs of the two water models are identical at $(T^{max}_{TMD},\rho^{max}_{TMD})$ as expected from the strong correlation between pair and tetrahedral ordering in the anomalous regime.

The distribution of tagged potential energies, $P(u_{tag})$, in rigid-body water models is approximately Gaussian, with a small asymmetric tail.[51,74,75] Unlike the tetrahedral order distributions, there is no prominent shoulder in the anomalous regime, as shown in Figure 7a for the $P(u_{tag})$ distribution for TIP4P water at 260 K and 1.00 g cm^{-3}.

To understand the contributions to u_{tag} from water molecules at different distances, we also compute the contribution to the tagged potential energy of a water molecule from water molecules restricted to lie in the first and second neighbor shells, denoted by u_{first} and u_{sec}, respectively. The cutoff distances for the first and second neighbor shells are taken as 3.5 Å and 5.5 Å, corresponding to the first and second minima in the $g_{OO}(r)$ pair correlation function, respectively, for TIP4P (see Figure 2b). Figure 3 shows the corresponding $P(u_{first})$ and $P(u_{sec})$ distributions. u_{first} is computed for a water molecule by summing the

Table 5. Comparison of Average Temperature and Average Pressure for the First 200 ps and Last 200 ps of the NVE Simulation of Peptide System Solvated with mTIP3P and TIP4P

water model	target temperature (K)	$\langle T_{first}\rangle$ (K)	$\langle T_{last}\rangle$ (K)	$\langle P_{first}\rangle$ (katm)	$\langle P_{last}\rangle$ (katm)
mTIP3P	300	301.48	301.86	0.0994	0.0844
	250	252.04	252.19	0.2487	0.2574
TIP4P	300	304.64	305.29	−0.1399	−0.1480
	250	252.91	253.72	0.0715	0.0837

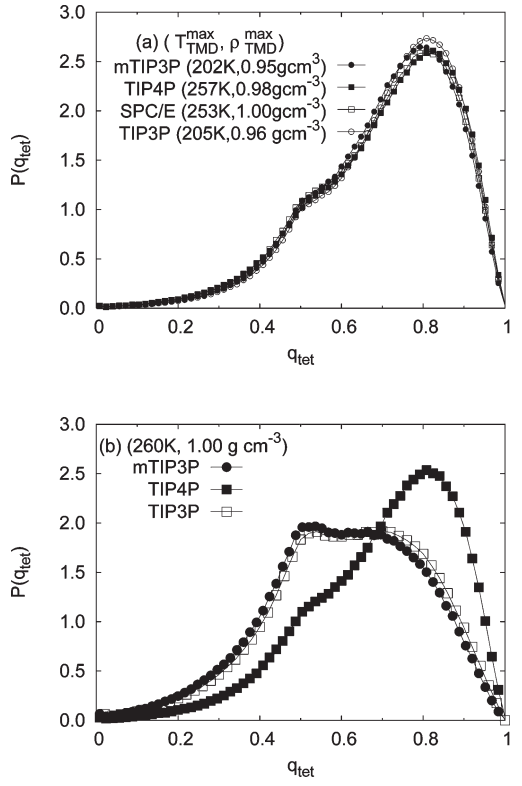

Figure 1. Normalized distributions of the tetrahedral order parameter (a) at the state point $(T^{max}_{TMD}, \rho^{max}_{TMD})$ corresponding to the maximum in temperature along the TMD locus for mTIP3P, TIP4P, SPC/E, and TIP3P water and (b) for mTIP3P, TIP4P, and TIP3P water at a common state point of (260 K, 1.00 g cm^{-3}).

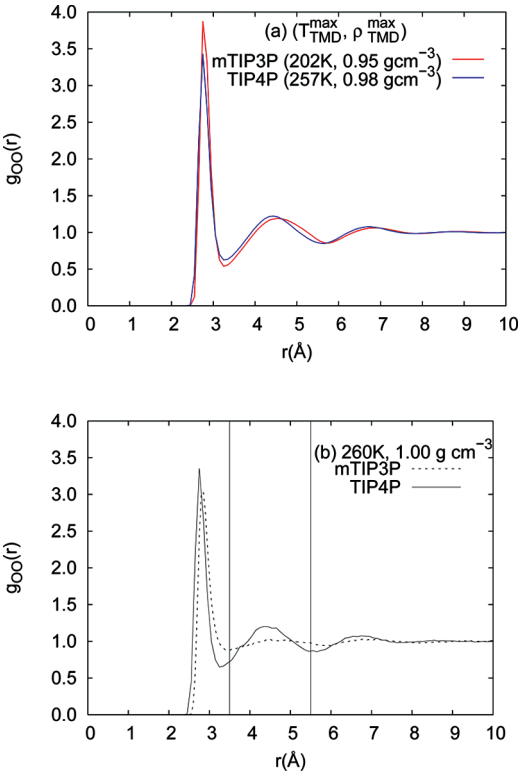

Figure 2. Radial distribution function of oxygen−oxygen, $g_{OO}(r)$, for mTIP3P and TIP4P water models at (a) their respective $(T^{max}_{TMD}, \rho^{max}_{TMD})$ state points and at (b) the state point (260 K, 1.00 g cm^{-3}). The positions of vertical lines on the x axis indicate the upper limit of the first and the second hydration shells from left to right, respectively.

interaction energy of that molecule with waters lying within the first hydration shell, i.e., within 3.5 Å for TIP4P at (260 K, 1.00 g cm^{-3}). Similarly, u_{sec} is computed for a water molecule by summing the interaction energy of that molecule with waters lying in the second shell, i.e., lying at a distance of 3.5−5.5 Å from that molecule. $u_{first+sec}$ is computed for a water molecule by summing the interaction energy of that molecule with all of the neighboring water molecules lying in both the first as well as the second shell of hydration, i.e., within 5.5 Å of that water molecule. So, $P(u_{first+sec})$ is the probability distribution of the $u_{first+sec}$ computed as above. Both the $P(u_{first})$ and $P(u_{sec})$ distributions are unimodal and do not show an obvious analogue of the strongly shouldered $P(q_{tet})$ distribution. The ensemble average of the combined contribution of the first and second neighbor shell corresponds to 92% of the ensemble-averaged TPE for TIP4P at (260 K, 1.00 g cm^{-3}), i.e., $\langle u_{first+sec}\rangle \approx \langle u_{tag}\rangle$ with molecules beyond the second shell contributing less than 10% to $\langle u_{tag}\rangle$. The ensemble-averaged value of TPE for TIP4P at (260 K, 1.00 g cm^{-3}) is −87.031 kJ mol^{-1}.

The coordination number (n) of a given water is the number of neighbors lying within 3.5 Å, ensuring that the next nearest neighbor lies beyond 3.5 Å.[76,77] The distribution of nearest neighbors in TIP4P and mTIP3P water at 260 K and 1.00 g cm^{-3} is shown in Figure 4a and b, respectively. In the case of TIP4P water at this state point, four- and five-coordination are almost equally probable, whereas in mTIP3P water, five-coordinate water molecules dominate. The average coordination number in TIP4P and mTIP3P water at this state point is 4.7 and 4.9, respectively. Neutron scattering data suggest that at 298 K and 1.00 g cm^{-3} each water molecule has ∼4.5 neighbors.[78]

3.1.2. Relationship between Local Order, Energy, and Coordination. It is evident that local order (q_{tet}), coordination number (n), and tagged molecule energy (u_{tag}) must carry correlated, but not identical, information about the local environment of water molecules. A simple correlation plot of the $q_{tet,i}$ and $u_{tag,i}$ for an individual molecule i sampled at a given state point, however, shows only very weak correlations between local order and energy. This lack of a well-defined relationship between the three quantities is also evident from the qualitatively different shapes of the shouldered $P(q_{tet})$ distributions compared with the unimodal $P(u_{tag})$ (Figure 7a) and $P(n)$ distributions (Figure 4).

Nonetheless, suitably defined averages of these quantities do show a good correlation. For example, the ensemble-averaged values of u_{tag} and q_{tet} along isochores have been shown to have a

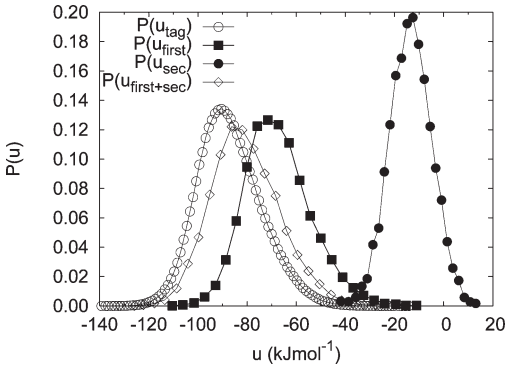

Figure 3. Normalized distributions of local energies of TIP4P water molecules at (260 K, 1.00 g cm^{-3}). The local energy is calculated as a sum of contributions from all other $N - 1$ molecules in the system and is denoted by u_{tag}. u_{first} and u_{sec} refer to local energies due to interactions with first and second shell neighbors, respectively; $u_{first+sec}$ refers to the combined contribution to local energy from the first and second shell neighbors.

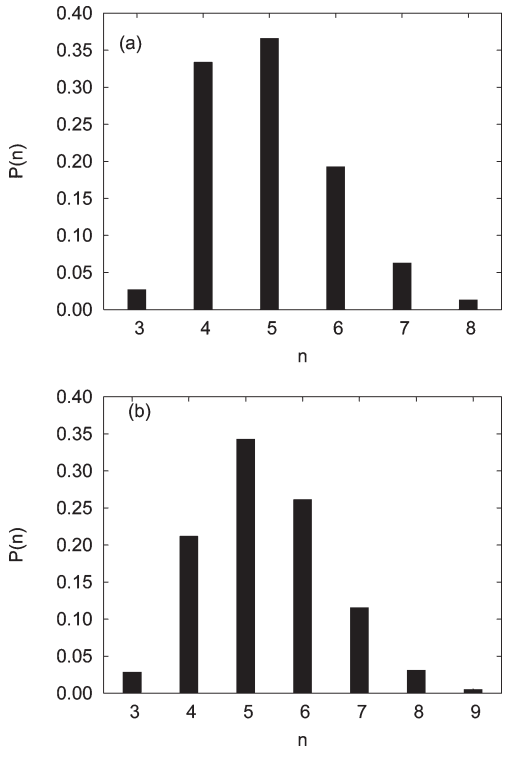

Figure 4. Coordination number distributions, $P(n)$, computed at (260 K, 1.00 g cm^{-3}) for (a) TIP4P and (b) mTIP3P. The probability of finding a higher coordination number ($n > 6$) of water is very low. $\Sigma_{n=1}^{8} P_n = 0.998$ for TIP4P and $\Sigma_{n=1}^{9} P_n = 0.997$ for mTIP3P.

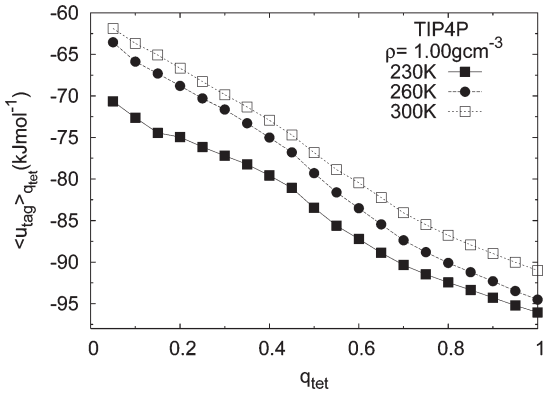

Figure 5. Correlations between local order and local energy averages for TIP4P water molecules at 1.00 g cm^{-3} and temperatures of 230, 260, and 300 K. The average local energy $\langle u_{tag} \rangle_{qtet}$ is calculated by averaging u_{tag} over molecules having q_{tet} values lying between q_{tet} and $q_{tet} + \delta q_{tet}$ ($\delta q_{tet} = 0.05$).

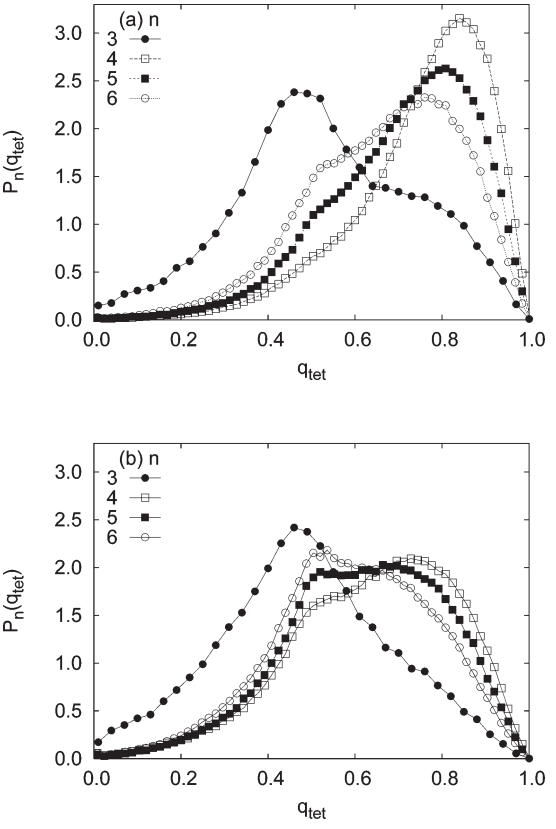

Figure 6. Normalized conditional probability distribution of local order, $P_n(q_{tet})$ for water molecules with coordination number (n) computed at (260 K, 1.00 g cm^{-3}) for (a) TIP4P and (b) mTIP3P.

well-defined linear correlation in previous studies.[51] Similarly, the tagged particle potential energy, $\langle u_{tag} \rangle_{qtet}$, obtained by averaging over water molecules with local tetrahedral order lying between q_{tet} and $q_{tet} + \delta q_{tet}$ shows a quasi-linear, negative correlation with q_{tet}.[73] In Figure 5, we show these correlations for selected state points of TIP4P water.

It is useful to employ other metrics in addition to correlation plots to characterize the relationships between local order, energy, and coordination number. We have found it convenient to use conditional distributions of one quantity subject to a restricted range of another quantity. For example, one can create distributions of the tetrahedral order and the TPE using only the subset of water molecules with coordination number n, which will be denoted by $P_n(q_{tet})$ and $P_n(u_{tag})$. Similarly one can consider the distributions, $P_u(q_{tet})$, corresponding to the distributions of q_{tet} for all molecules with tagged potential energy lying between u and $u + \delta u$ where u is very small compared with the range of accessible values of u.

dx.doi.org/10.1021/ct2002732 |J. Chem. Theory Comput. 2011, 7, 3354–3367

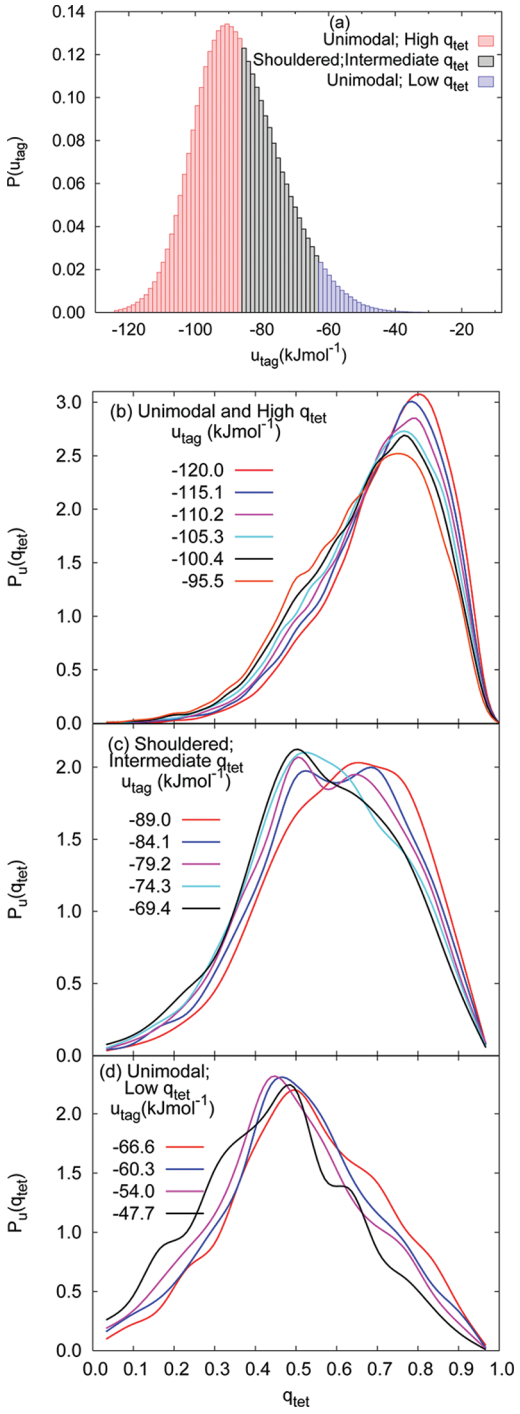

Figure 7. Relationship between tagged molecule potential energy distribution, $P(u_{tag})$, and tetrahedral order distribution, $P_u(q_{tet})$, conditional on water molecules having u_{tag} lying between u and $u + du$. Results are shown for TIP4P water at (260 K, 1.00 g cm^{-3}). Part a shows a normalized $P(u_{tag})$ distribution (δu = 0.7 kJ mol^{-1}) colored according to three types of normalized $P_u(q_{tet})$ distributions shown in parts b, c, and d. Part b shows unimodal $P_u(q_{tet})$ distributions for water molecules with high q_{tet} having $-120 \le u_{tag} \le -90$ kJ mol^{-1}. Part c shows strongly shouldered $P_u(q_{tet})$ distributions for molecules with intermediate q_{tet} having $-90 \le u_{tag} \le -65$ kJ mol^{-1}. Part d shows unimodal $P_u(q_{tet})$ distributions for water with a nontetrahedral environment having $-65 \le u_{tag} \le -40$ kJ mol^{-1}. The red, black, and blue regions of $P(u_{tag})$ distribution correspond to water molecules having $P_u(q_{tet})$ distributions shown in parts b, c, and d, respectively.

Figure 6 shows the conditional tetrahedral order distributions, $P_n(q_{tet})$, for TIP4P and mTIP3P water at 260 K and 1.00 g cm^{-3}. In the case of TIP4P water, it is immediately obvious that the four-coordinate molecules are preferentially in a strongly tetrahedral environment. The $P_{n=4}(q_{tet})$ distribution is unimodal with a sharp peak at $q_{tet} \approx 0.8$. The five- and six-coordinate water molecules show shouldered $P(q_{tet})$ distributions with a shoulder at $q_{tet} \approx 0.45$. The three-coordinate water molecules, which form only a 0.029 fraction of water molecules, are far from tetrahedrality having unimodal $P(q_{tet})$ distribution with a peak at $q_{tet} \approx 0.4$. In the case of mTIP3P water, the $P_{n=3}(q_{tet})$ distribution is very similar to that of TIP4P. The conditional tetrahedral order distributions for n = 4, 5, and 6 are very similar, shouldered distributions with peaks at $q_{tet} \approx 0.5$ and $q_{tet} \approx 0.7$ of almost equal height.

Figure 7a shows the $P(u_{tag})$ distribution of TIP4P water at (260 K, 1.00 g cm^{-3}) subdivided into histogram bins of approximately 1 kJ mol^{-1} width. The $P_u(q_{tet})$ distributions in each bin were generated and could be classified into three types (Figure 7b−d). For the low TPE histograms, lying in the range of −120 to −90 kJ mol^{-1}, the $P_u(q_{tet})$ distributions are unimodal with a dominant peak corresponding to a strongly tetrahedral local environment at $q_{tet} \approx 0.85$ and a weak shoulder at approximately $q_{tet} \approx 0.5$. Comparison with Figure 6a suggests that water molecules in this energy region are four-coordinated. Water molecules with u_{tag} values in the range of −90 to −65 kJ mol^{-1} have local environments of intermediate tetrahedrality. $P_u(q_{tet})$ distributions for these water molecules have a peak at $q_{tet} \approx 0.75$ and a second one at $q_{tet} \approx 0.45$. Both peaks are of comparable height, with the $q_{tet} \approx 0.45$ peak becoming more prominent with increasing u_{tag}. The water molecules in the high energy tail of the u_{tag} distribution (−65 to −40 kJ mol^{-1}) have nontetrahedral local environment with unimodal $P_u(q_{tet})$ distributions having a peak lying below ∼0.43. Thus, it is possible to color the histogram bins in the $P(u)$ distributions in terms of three qualitatively different types of $P_u(q_{tet})$ distributions: (i) strongly tetrahedral with a sharp peak for q_{tet} lying between approximately 0.8 and 0.9, (ii) intermediate tetrahedral character with significant proportion of tetrahedral and nontetrahedral environments, and (iii) nontetrahedral distributions with a peak at q_{tet} of about 0.5. The tetrahedral order distributions conditional on a particular value of the tagged particle energy show that TIP4P water molecules with low local energies will exist preferentially in tetrahedral environments, illustrating the energetic bias for terahedrality for this model at the given state point.

Figure 8 shows the conditional $P_u(q_{tet})$ for mTIP3P water at 260 K and 1.00 g cm^{-3} . In striking contrast to the results for TIP4P, the $P_u(q_{tet})$'s are essentially identical for the entire range of u_{tag} values and consist of distributions indicating comparable proportions of tetrahedral and nontetrahedral local environments. In the case of mTIP3P, there is no energetic bias for tetrahedrality at a temperature of 260 K.

The shouldered distributions of $P(q_{tet})$ in the anomalous regime of the water models show that the free energy of the system as a function of local order must have two local minima. Since the local energy distributions do not show a corresponding presence of tetrahedral and nontetrahedral environments, one expects that entropic factors must play an important role. In a recent work, Stanley and co-workers introduced an entropy measure based on the tetrahedral order distribution .[79] We adapt it to define an entropy measure, $S_q(u_{tag})$, using the conditional $P_u(q_{tet})$ distribution for all water molecules with u_{tag} lying

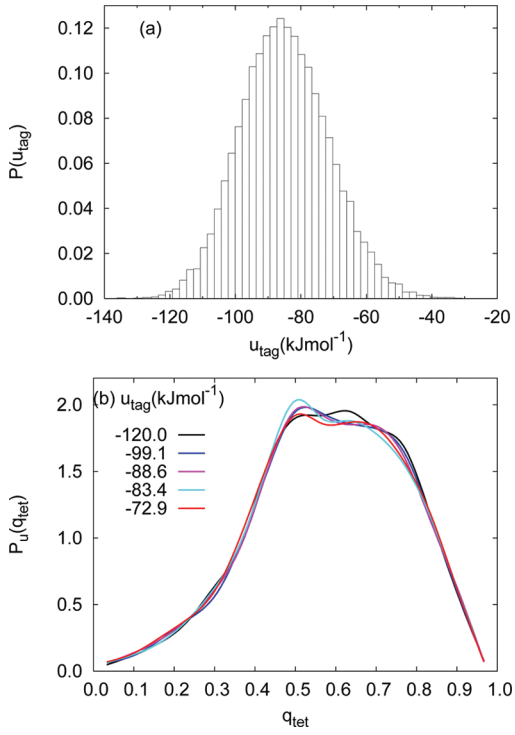

Figure 8. Relationship between tagged molecule potential energy distribution, $P(u_{tag})$, and tetrahedral order distribution, $P_u(q_{tet})$, conditional on water molecules having u_{tag} lying between u and $u + du$. Results are shown for mTIP3P water at (260 K, 1.00 g cm^{-3}). Part a shows normalized $P(u_{tag})$ distribution (δu = 1.05 kJ mol^{-1}). Part b shows $P_u(q_{tet})$ distributions for water molecules with u_{tag} lying between u and $u + \delta u$ for the entire range of u_{tag} shown in part a. mTIP3P does not show different types of $P_u(q_{tet})$ distributions for different ranges of u_{tag} at this state point as are shown by TIP4P (Figure 7b–d).

between u and $u + du$ at a given state point.

$$S_q(u_{tag}) = S_0 + \frac{3}{2}k_B \int_{q_{tet}^{min}}^{q_{tet}^{max}} \ln(1 - q_{tet})\, P_u(q_{tet})\, dq_{tet} \quad (3)$$

$S_q(u_{tag})$ is measured relative to S_0 where $S_0 = k_B[\ln \Omega_0 + 3/2 \ln(8/3)]$ at all state points.[79] The q_{tet}^{min} and q_{tet}^{max} correspond to the minimum and maximum values of q_{tet} of water molecules having u_{tag} in the range of u and $u + \delta u$. $S_q(u_{tag})$ is calculated in different ranges of u_{tag} described above, and its behavior is examined as a function of u_{tag} for mTIP3P and TIP4P (see Figure 9).

It is observed that for TIP4P at (260 K, 1.00 g cm^{-3}), $S_q(u_{tag})$ shows a positive correlation with u_{tag} and anticorrelation with q_{tet}, indicating that the higher the q_{tet}, the more negative is the tetrahedral entropy, and the lower the u_{tag}, the lower is the tetrahedral entropy of the system. At 350 K and 1.00 g cm^{-3} for TIP4P water, the correlation is somewhat weaker. For mTIP3P, there is no correlation between $S_q(u_{tag})$ and u_{tag} at 260 K. At the maximum temperature along the TMD locus, the $S_q(u_{tag})$ plots for mTIP3P and TIP4P are very similar.

3.2. Tetrahedral Order and Local Energetics of Water in Hydration Shells. Figure 10 compares the average number of water molecules $n(r)$ present at a distance between r and $r + \delta r$ (δr = 0.25 Å) from the β-hairpin peptide solvated in mTIP3P and TIP4P water at 250 and 300 K. The distance of the water molecule was measured relative to the nearest atom of the

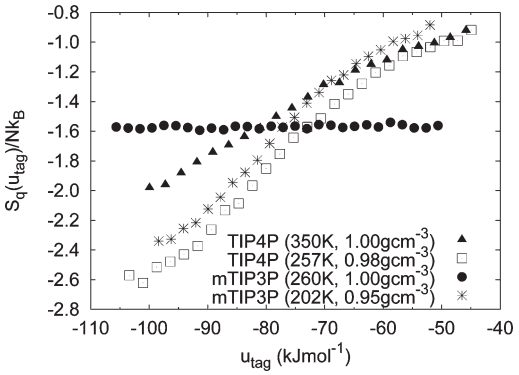

Figure 9. Plot of tetrahedral entropy, $S_q(u_{tag})$, defined in eq 3 as a function of u_{tag} for mTIP3P and TIP4P at various state points. (T_{TMD}^{max}, ρ_{TMD}^{max}) for mTIP3P is (202 K, 0.95 g cm^{-3}) and for TIP4P is (257 K, 0.98 g cm^{-3}).

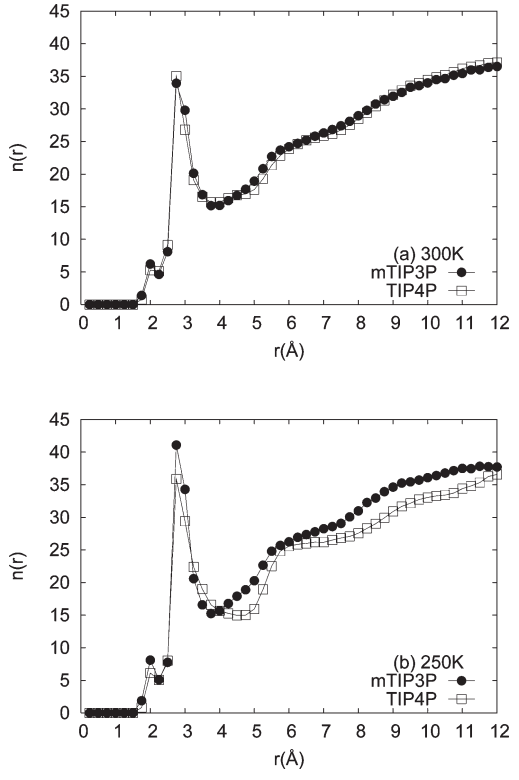

Figure 10. Comparison of the number of water molecules, $n(r)$, as a function of distance r from 2GB1 β-hairpin peptide when solvated in mTIP3P and TIP4P water at (a) 300 K and (b) 250 K.

peptide. At 300 K, $n(r)$ does not change significantly with the change in water models, mTIP3P and TIP4P, in agreement with previous studies.[50] At 250 K, small differences between the solvent models can be seen in the neighborhood of the first hydration shell, with a sharper peak coming from the mTIP3P model. A weak layering effect which extends up to 12 Å from the peptide is seen for both the water models.[80]

Figure 11 shows the radial variation of the tagged potential energy as a function of the distance from the β-hairpin peptide at 300 and 250 K for both water models. The $u_{tag}(r)$ curves are generated by calculating the mean u_{tag} values of all of the $n(r)$ water molecules lying at a distance between r and $r + \delta r$ from the

dx.doi.org/10.1021/ct2002732 |J. Chem. Theory Comput. 2011, 7, 3354–3367

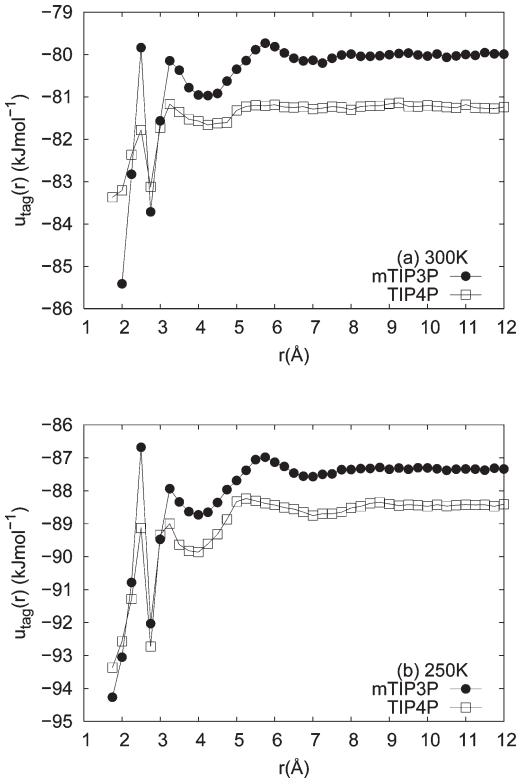

Figure 11. Comparison of tagged potential energy of water molecules, $u_{tag}(r)$, as a function of the distance (r) from the 2GB1 β-hairpin peptide when solvated in mTIP3P and TIP4P water at (a) 300 K and (b) 250 K. The value of $u_{tag}(r)$ at 12 Å is close to the bulk $\langle u_{tag}\rangle$ value at 1.00 g cm^{-3}. The values of $\langle u_{tag}\rangle$ at 1.00 g cm^{-3} are -81.88 kJ mol^{-1} and -81.29 kJ mol^{-1} for TIP4P and mTIP3P at 300 K, respectively, and -88.41 kJ mol^{-1} and -86.30 kJ mol^{-1} for TIP4P and mTIP3P at 250 K, respectively.

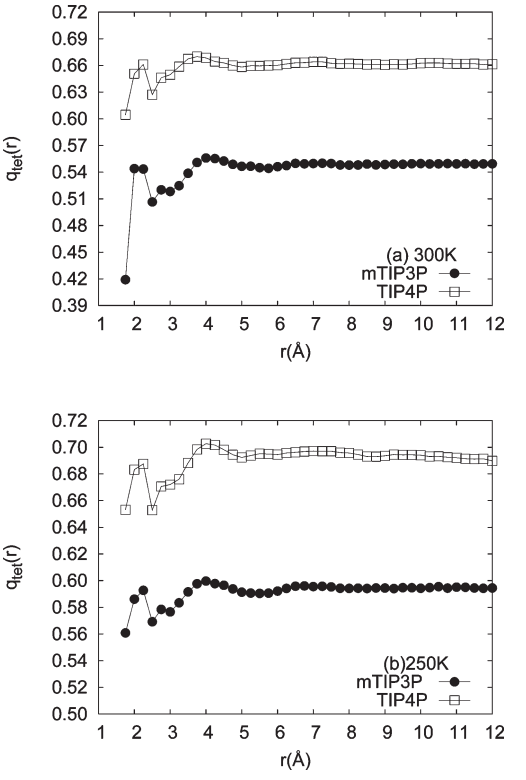

Figure 12. Comparison of tetrahedral order, $q_{tet}(r)$, as a function of distance (r) from the 2GB1 β-hairpin peptide when solvated in mTIP3P and TIP4P water at (a) 300 K and (b) 250 K.

peptide. Our previous study shows an oscillatory variation in $u(r)$ beyond the first hydration shell in mTIP3P water.[51] The oscillatory behavior of TIP4P water is very similar to that of mTIP3P solvent, except that the oscillations are less pronounced in TIP4P. The $u_{tag}(r)$ values are lower for the TIP4P model by approximately 1 kJ mol^{-1} at both 300 and 250 K.

Figure 12 shows the tetrahedral order parameter as a function of the distance from the peptide. As discussed in our previous study, beyond the first hydration shell, the maxima and minima in the $q_{tet}(r)$ distribution tend to be anticorrelated with those in $u_{tag}(r)$.[51] As expected on the basis of bulk behavior, TIP4P solvent shows significantly higher local tetrahedral order compared with the mTIP3P solvent in the hydration shell of a peptide.

The results presented in Figures 10−12 focus on the local energy and structure beyond the first hydration shell. Within the first hydration shell, we expect the tetrahedral network of water to be distorted, in addition to a strong dependence on the chemical character of the residues.

To characterize the differences between the two water models within this critical solvent layer, Figure 13 shows mean TPEs of water molecules lying within 5 Å of any atom of each amino acid residue. The variation in TPE as a function of the residues of the peptide shows similar qualitative behavior for both mTIP3P and TIP4P water models; i.e., the water molecules near hydrophilic residues 42(Glu), 46(Asp), 47(Asp), and 56(Glu) have lower TPEs and those near hydrophobic residues 43(Trp) and 52-(Phe) have higher TPE values at 300 K. The quantitative

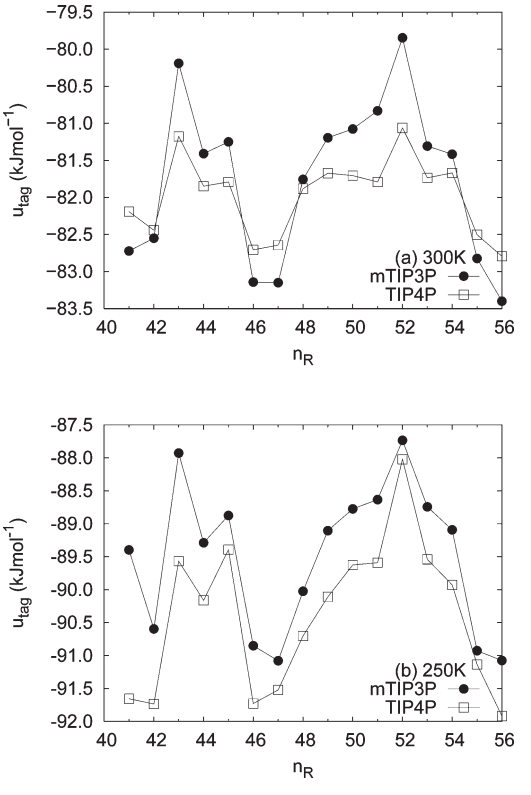

Figure 13. Residue-wise dependence of tagged potential energy for mTIP3P and TIP4P at (a) 300 K and (b) 250 K.

dx.doi.org/10.1021/ct2002732 |J. Chem. Theory Comput. 2011, 7, 3354–3367

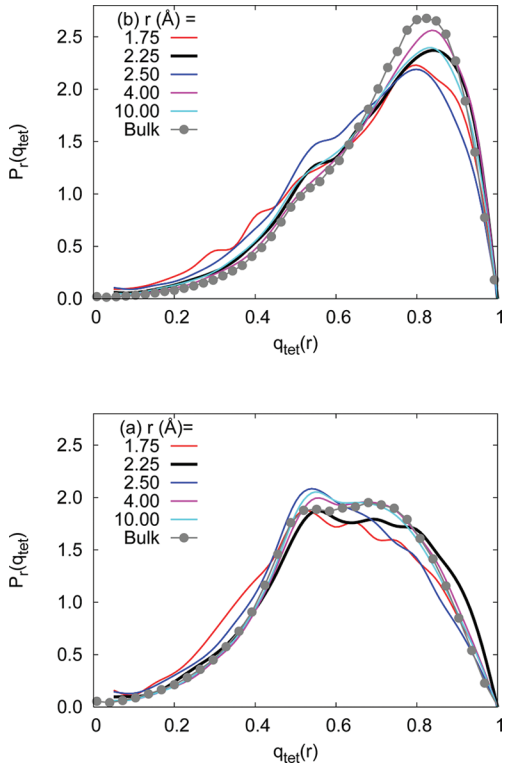

Figure 14. Normalized distributions of tetrahedral order, $P_r(q_{tet})$, for water molecules lying between a distance of r and $r + \delta r$ (δr = 0.25 Å) from the peptide solvated in (a) mTIP3P and (b) TIP4P at 250 K. The bulk $P(q_{tet})$ distributions shown correspond to the state point (250 K, 1.00 g cm^{-3}) for both the water models.

differences in TPE of the water molecules near the hydrophilic and hydrophobic residues are, however, greater in the case of mTIP3P than in TIP4P.

Figure 14 shows the $P_r(q_{tet})$ distributions for water molecules lying between a distance of r and $r + \delta r$ of the peptide solvated in mTIP3P as well as TIP4P water at 250 K. The $P_r(q_{tet})$'s are compared with the bulk $P(q_{tet})$ distributions of the two water models. The distances corresponding to minima in the $q_{tet}(r)$ distributions shown in Figure 12 show tetrahedral order distributions with somewhat higher probabilities of low q_{tet} values. It is evident that deviations from the bulk distribution are small as a function of the distance from the peptide. It should be noted that q_{tet} has been defined to include the four nearest heavy atoms, whether they belong to water or the peptide. Since the oxygen atom in water will tend to form two donor and two acceptor hydrogen bonds, this definition of q_{tet} assumes that replacement of water−water hydrogen bonds with other hydrogen bonds (e.g., water and hydroxyl group of side chain) does not significantly alter the local environment of a water molecule. The distortion in the tetrahedral network of the water molecules in the first hydration shell is not as severe as expected, even though the TPE values of water molecules in the first hydration shell are significantly lower. It should be noted that similar small perturbations of the tetrahedral order distribution as a function of the radial distance from the solute were seen in the case of aqueous sugar solutions.[81]

4. CONCLUSIONS

We show that the relationship between tetrahedral order and anomalous behavior is very similar in the rigid-body water models (TIP3P, mTIP3P, SPC/E, and TIP4P); for example, the tetrahedral order distributions for mTIP3P, TIP4P, and SPC/E water are superimposable at the state point (T_{TMD}^{max}, ρ_{TMD}^{max}) corresponding to the maximum temperature for onset of the density anomaly. The energetic stabilization of terahedrality for the different water models can vary widely, as indicated by the wide variation in the temperature regimes of the anomalies. In the temperature range of 250−300 K, of interest in biomolecular simulations, the mTIP3P water model behaves as a normal liquid, while the TIP4P water model is an anomalous, tetrahedral liquid. To understand the relationship between local order (q_{tet}), local energy (u_{tag}), and local coordination number (n) in these two water models, we construct tetrahedral order distributions conditional on a specific value of the coordination number or a narrow range of tagged molecule potential energies. The $P_n(q_{tet})$ distributions are obtained by averaging over all molecules with exactly n neighbors in the first coordination shell. The $P_u(q_{tet})$ distributions are obtained by averaging over all water molecules with TPE lying between u and $u + \delta u$. The $P_n(q_{tet})$ or $P_u(q_{tet})$ for TIP4P can be classified into three types: (i) strongly tetrahedral with a sharp peak for q_{tet} lying between 0.8 and 0.9, (ii) intermediate tetrahedral character with a broad plateau or strong shoulder indicating a significant proportion of both tetrahedral and nontetrahedral environments, and (iii) nontetrahedral distributions with a peak at q_{tet} of about 0.5. Using the conditional distributions, we show that four-coordinate environments in TIP4P water in the 250−270 K regime are likely to be strongly tetrahedral with lower local tagged molecule potential energies. Higher coordination sites will have lower tetrahedrality and higher local energy. The mTIP3P model of bulk water in the same temperature regime displays no energetic bias toward tetrahedral local environments. The tendency of water molecules with different binding energies (TPEs) to occupy environments with different degrees of disorder can be effectively illustrated by constructing entropy measures based on the $P_u(q_{tet})$ distributions. At the maximum temperature along the TMD locus, the correlation between tetrahedral entropy versus tagged potential energy is strong and virtually identical for mTIP3P and TIP4P. In TIP4P, this correlation is retained up to temperatures as high as 300 K, while it is lost by 250 K in mTIP3P.

We compare the effect of solvating the 16-residue β-hairpin fragment of 2GB1 in mTIP3P and TIP4P solvents. The hydration shell coordination profile ($n(r)$) of the number of water molecules at a distance r from the peptide is almost identical in the two solvents at 300 K, though lowering of the temperature to 250 K increases the differences slightly. This is consistent with earlier studies by Nutt and Smith on the radial distribution functions in water.[50] The differences between the two solvent models are larger, however, for the tagged potential energy ($u_{tag}(r)$) as a function of distance r from the peptide, though the weak oscillatory variation as a function of r is qualitatively very similar in the two solvents. The residue-wise variation in the tagged potential energy of water molecules within the first hydration shell is qualitatively similar in the two models. The differences between the two solvent models are larger when the radial distribution of the tetrahedral order is monitored, compared to the tagged potential energy. This difference, however, seems to originate from the differences in the bulk tetrahedral order distributions of the solvent at the same state point since perturbation in the local tetrahedral order distributions of the bulk solvent due to the presence of the solute is marginal.

To summarize, the mTIP3P and TIP4P water models show qualitatively different behavior in terms of the relationship between tetrahedral order and local energy that governs the thermodynamic anomalies in the 250−300 K temperature regime. As solvents in the neighborhood of a biomolecular solute, the differences between the two models, however, are quantitative rather than qualitative.

It is useful to place our results in the context of previous work on structure and energetics in bulk water and in aqueous solutions. We show that local order, energy, and coordination number in bulk water show similar but not identical behavior in the context of the liquid-state anomalies. This is consistent with the multiple time-scale behavior seen in the time correlation of local fluctuations in tetrahedral order, coordination number, and tagged particle potential energies.[7,56,57,76,82] Our results for the differences in shapes of tetrahedral order distributions for water molecules with different local coordination are also consistent with the recent work of Netz and co-workers that density−density correlations do not have a simple relationship with spatial correlations in structural order.[83] Previous studies suggest that rigid-body water models that provide a more accurate phase diagram and equation of state, also prove to be more reliable for studying solvation and clathrate formation of small hydrophobes.[26,27] A systematic comparison of hydration behavior of amino acid analogues, small solutes, and proteins (e.g., myoglobin and crambin) predicted by different biomolecular force fields and water models suggests that qualitative trends are similar, though the equation of state of the water model strongly influences the hydration enthalpy.[31,49,50] These results are consistent with our observations on the hydration shell structure and energetics of the 2GB1 peptide in water.

The results of this study provide some insight into the role played by different components of the intermolecular interactions of water in controlling hydration behavior, which should help in the appropriate design of coarse-grained models for water.[84−86] A crucial factor controlling the chemical potential of small hydrophobes in water is the cavity distribution function which depends on the size of the water molecules.[27,28] In the TIPnP water models, this aspect will be controlled essentially by the Lennard-Jones size parameter and will be identical for all of them. The geometry of the partial charges is the crucial difference between the two models studied here. As pointed out by Vega and others, the dipole moments of most rigid-body water models are very similar, though the quadrupole moments are significantly different.[40,61] The similar dipole moments of the two models studied here imply that the most important contribution to solvation of polar solutes or amino acid side chains is similar in the mTIP3P and TIP4P models. The dipole−quadrupole ratio has been shown to be crucial in determining the phase diagram and equation of state of water, especially the regions of stability of the different ice phases.[61] One may therefore surmise that this factor will affect organization of the tetrahedral network and therefore the presence of water-like anomalies, solvation of small hydrophobes, and clathrate formation.[26,27] Given the length-scale dependence of hydrophobicity, the dipole−quadrupole ratio and the associated tetrahedral hydrogen-bonded network structure may play a relatively small role in the hydration of a peptide of nanoscale dimensions with a heterogeneous set of charged, polar, and nonpolar residues, as suggested by our results. The qualitatively similar behavior in local energy and order in the peptide hydration shell in mTIP3P and TIP4P water shown by us leads to the conclusion that the dipole moment and the van der Waals radius play a crucial role in determining overall trends in hydration properties, while the dipole−quadrupole ratio and equation of state of water play a subsidiary though significant role.

APPENDIX A: EVALUATION OF TAGGED MOLECULE POTENTIAL ENERGY FOR PAIR-ADDITIVE POTENTIALS

In this section, we present the equations required in order to evaluate the tagged molecule potential energy (TPE or u), defined as the interaction of a given molecule with all other molecules in the system. Our equations apply to the case where intermolecular forces are modeled using pair interactions between Lennard-Jones and charge sites and do not take into account intramolecular contributions. The Coulombic interactions are evaluated using Ewald summation. Regarding computational details, we have computed the TPE of water molecules in rigid-body models of bulk water using these equations by adapting standard Ewald summation codes.[88] We have then shown that the TPE can be computed by relatively small modifications of the DL_POLY source code. The *pairInteraction* command in the NAMD input file was then used to also compute the TPE distributions for bulk water and was shown to give essentially identical results, though NAMD uses the particle-mesh Ewald method to evaluate the Coulombic forces. With this validation, we could use the *pairInteraction* command in NAMD to compute the TPEs of water molecules in the hydration shell of a biomolecule.

In the case of pair-additive potential models, such as the CHARMM biomolecular force field, the intermolecular contribution to the potential energy (U_{inter}) can be written as a sum of the Coulombic (U_{Coul}) and van der Waals (U_{vdW}) interactions.

$$U_{\text{inter}} = U_{\text{Coul}} + U_{\text{vdW}} \tag{A.1}$$

In the Ewald summation, U_{Coul} is written as

$$U_{\text{Coul}} = U_{\text{screen}} + U_{\text{rec}} - U_{\text{self}} \tag{A.2}$$

where U_{screen} is the real space contribution from screened charges, U_{rec} is the reciprocal space contribution, and U_{self} is the self-interaction correction.[64,87,88] The tagged molecule potential energy (TPE) of the ith molecule will therefore contain a corresponding set of contributions and will be written as

$$u_i = u_i^{\text{screen}} + u_i^{\text{rec}} - u_i^{\text{self}} + u_i^{\text{vdW}} \tag{A.3}$$

In the case of the one-component bulk water system, the tagged molecule energies will satisfy the relation

$$U_{\text{inter}} = \frac{1}{2}\sum_i u_i \tag{A.4}$$

The rigid-body models associate a set of Lennard-Jones (LJ) and charged sites with a water molecule.

The TPE contribution due to van der Waals interactions will therefore be

$$u_i^{\text{vdW}} = \sum_k^{N_{\text{LJ}}} u_k^{\text{vdw}} = \sum_k^{N_{\text{LJ}}}\sum_j u_{\text{LJ}}(r_{kj}) \tag{A.5}$$

where the sum over k represents summation of over all N_{LJ} Lennard-Jones sites on molecule i and the sum over j is the interaction of LJ site k with all LJ sites not on molecule i.

In the case of Ewald summation, it is necessary to consider the interaction of each of the charge sites l with all other charge sites not on the same molecule. Ewald summation replaces the bare charges by screened Gaussian charge distributions to give a real-space contribution to the potential energy, written as

$$U_{\text{screen}} = \frac{1}{2}\sum_{i=1}^{N}\sum_{j=1}^{N}\frac{q_i q_j}{4\pi\varepsilon_0}\frac{\text{erfc}(\alpha|r_{ij}|)}{|r_{ij}|} \tag{A.6}$$

$$= \frac{1}{2}\sum_{j=1}^{N} u_j^{\text{creal}} \tag{A.7}$$

where u_j^{creal} is the interaction of a screened charge site with all other screened charges. The u_i^{screen} contribution to the TPE of the ith molecule must be computed by summing the u_j^{creal} contributions due to all N_C charged sites on molecule i.

The reciprocal-space contribution to the Coulombic energy, U_{rec}, is written as

$$U_{\text{rec}} = \frac{1}{2V_0\varepsilon_0}\sum_{|k|\neq 0}^{\infty}\frac{\exp(-k^2/4\alpha^2)}{k^2}\left|\sum_{j}^{N} q_j \exp(-i\mathbf{k}\cdot\mathbf{r}_j)\right|^2 \tag{A.8}$$

where j labels the charge sites in the system. By replacing the squared modulus term by a double sum over i and j, we can write

$$U_{\text{rec}} = \frac{1}{2V_0\varepsilon_0}\sum_{|k|\neq 0}^{\infty}\frac{\exp(-k^2/4\alpha^2)}{k^2}\sum_{j=1}^{N}\sum_{i=1}^{N} q_i q_j \exp(-i\mathbf{k}\cdot(\mathbf{r}_j-\mathbf{r}_i)) \tag{A.9}$$

By rearranging, one can show that it is possible to write U_{rec} as a sum of contributions from each charge site j of the form

$$U_{\text{rec}} = \frac{1}{2}\sum_{j=1}^{N} u_j^{\text{crec}} \tag{A.10}$$

where u_j^{crec} is the reciprocal space contribution to the energy of interaction of a charge site with all other charges in the system and may be explicitly written as

$$u_j^{\text{crec}} = \frac{1}{V_0\varepsilon_0}\sum_{|k|\neq 0}^{\infty} q_j \exp(-i\mathbf{k}\cdot\mathbf{r}_j)\frac{\exp(-k^2/4\alpha^2)}{k^2}\sum_{i=1}^{N} q_i \exp(i\mathbf{k}\cdot\mathbf{r}_i) \tag{A.11}$$

The u_i^{rec} contribution to the TPE of the ith molecule must be computed by summing the u_j^{crec} contributions due to all N_C charged sites on molecule i.

The self-interaction term U_{self} corrects for the spurious interaction energy in U_{rec} of each screened charge distribution with itself as well as removes the interactions between charged sites on the same molecules. For a molecule i, this term can be written as

$$u_i^{\text{self}} = \frac{1}{4\pi\varepsilon_0}\sum_{l\leq m}^{N_C}\left(q_l q_m \delta_{lm}\frac{\alpha}{\sqrt{\pi}} + \frac{\text{erf}(\alpha r_{\text{lm}})}{r_{lm}^{1-\delta_{lm}}}\right) \tag{A.12}$$

where l and m label charge sites on the same molecule i and N_C is the number of charge-carrying sites per molecule.

AUTHOR INFORMATION

Corresponding Author

*Tel.: (+)91-11-2659-1510. Fax: (+)91-11-2686-2122. E-mail: charus@chemistry.iitd.ernet.in.

ACKNOWLEDGMENT

This work was financially supported by the Department of Science and Technology, New Delhi. D.N. would like to thank the Council of Scientific and Industrial Research for the award of a Junior Research Fellowship. M.A. would like to thank the Indian Institute of Technology—Delhi for the award of a Senior Research Fellowship. C.C. and D.N. would like to thank Sanjoy Bandhyopadhyay and Sudipta Kumar Sinha for useful discussions.

REFERENCES

(1) Dill, K.; Truskett, T.; Vlachy, V.; Hribar-Lee, B. Modelling water, the hydrophobic effect and ion solvation. *Annu. Rev. Biophys. Biomol. Struct.* **2005**, *34*, 173–199.

(2) Chandler, D. Interfaces and the driving force of hydrophobic assembly. *Nature* **2005**, *437*, 640–647.

(3) Ball, P. Water as an active constituent in cell biology. *Chem. Rev.* **2008**, *108*, 74–108.

(4) Debenedetti, P. G. Supercooled and glassy water. *J. Phys., Cond. Matt.* **2003**, *15*, 1669–1726.

(5) Bellissent-Funel, M.-C. *Hydration Processes in Biology: Theoretical and Experimental Approaches*; IOS Press: Amsterdam, The Netherlands, 1999.

(6) Li, Z.; Lazaridis, T. Water at biomolecular binding interfaces. *Phys. Chem. Chem. Phys.* **2007**, *9*, 573–581.

(7) Mishima, O.; Stanley, H. E. The relationship between liquid, supercooled and glassy water. *Nature* **1998**, *396*, 329–335.

(8) Chaplin, M. The Anomalous Properties of Water. http://www.lsbu.ac.uk/water/anmlies.html (accessed Jul 30, 2011).

(9) Hansen, J.-P.; McDonald, I. *Theory of Simple Liquids*, 3rd ed.; Elsevier: New York, 2006.

(10) Angell, C. A.; Bressel, R. D.; Hemmati, M.; Sarec, E. J.; Tuckerd, J. C. Water and its anomalies in perspective: tetrahedral liquids with and without liquid - liquid phase transitions. *Phys. Chem. Chem. Phys.* **2000**, *2*, 1559–1566.

(11) Errington, J. R.; Debenedetti, P. G. Relationship between structural order and the anomalies of liquid water. *Nature* **2001**, *409*, 318–321.

(12) Sharma, R.; Chakraborty, S. N.; Chakravarty, C. Entropy, diffusivity, and structural order in liquids with waterlike anomalies *J. Chem. Phys.* **2006**, *125*, 204501.

(13) Agarwal, M.; Sharma, R.; Chakravarty, C. Ionic melts with waterlike anomalies: Thermodynamic properties of liquid BeF_2. *J. Chem. Phys.* **2007**, *127*, 164502.

(14) Agarwal, M.; Chakravarty, C. Waterlike Structural and Excess Entropy Anomalies in Liquid Beryllium Fluoride. *J. Phys. Chem. B* **2007**, *111*, 13294–13300.

(15) Sharma, R.; Agarwal, M.; Chakravarty, C. Estimating the entropy of liquids from atom-atom radial distribution functions: silica, beryllium fluoride and water. *Mol. Phys.* **2008**, *106*, 1925–1938.

(16) Mittal, J.; Errington, J. R.; Truskett, T. M. Relationship between thermodynamics and dynamics of supercooled liquids. *J. Chem. Phys.* **2006**, *125*, 076102.

(17) Jabes, B. S.; Agarwal, M.; Chakravarty, C. Tetrahedral order, pair correlation entropy, and waterlike liquid state anomalies: Comparison of GeO_2 with BeF_2, SiO_2, and H_2O. *J. Chem. Phys.* **2010**, *132*, 234507.

(18) Agarwal, M.; Singh, M.; Sharma, R.; Alam, M. P.; Chakravarty, C. Relationship between Structure, Entropy, and Diffusivity in Water and Water-Like Liquids. *J. Phys. Chem. B* **2010**, *114*, 651–659.

(19) Chopra, R.; Truskett, T. M.; Errington, J. R. On the use of excess entropy scaling to describe the dynamic properties of water *J. Phys. Chem. B* **2010**, *114*, 10558–10566.

(20) Hujo, W.; Jabes, B. S.; Rana, V. K.; Chakravarty, C.; Molinero, V. The Rise and Fall of Anomalies in Tetrahedral Liquids. 2011, arXiv:1107.5623v1 [cond-mat.soft]. http://arxiv.org/abs/1107.5623 (accessed Jul 29, 2011).

(21) Molinero, V.; Sastry, S.; Angell, C. A. Tuning of Tetrahedrality in a Silicon Potential Yields a Series of Monatomic (Metal-like) Glass Formers of Very High Fragility. *Phys. Rev. Lett.* **2007**, *97*, 075701.

(22) Angell, C. A.; Kanno, H. Density Maxima in High-Pressure Supercooled Water and Liquid Silicon Dioxide. *Science* **1976**, *193*, 1121–1122.

(23) Sciortino, F.; Poole, P. H.; Essmann, U.; Stanley, H. E. Line of compressibility maxima in the phase diagram of supercooled water. *Phys. Rev. E* **1997**, *55*, 727–737.

(24) Scala, A.; Starr, F.; La Nave, E.; Stanley, H.; Sciortino, F. Free energy surface of supercooled water. *Phys. Rev. E* **2000**, *62*, 8016–8020.

(25) Abascal, J. L. F.; Vega, C. Widom line and the liquid-liquid critical point for the TIP4P/2005 water model. *J. Chem. Phys.* **2010**, *133*, 234502.

(26) Paschek, D. Temperature dependence of the hydrophobic hydration and interaction of simple solutes: An examination of five popular water models. *J. Chem. Phys.* **2004**, *120*, 6674–6690.

(27) Lynden-Bell, R.; Giovambattista, N.; Debenedetti, P.; Head-Gordon, T.; Rossky, P. Hydrogen bond strength and network structure effects on hydration of non-polar molecules. *Phys. Chem. Chem. Phys.* **2011**, *13*, 2748–2757.

(28) Hummer, G.; Garde, S.; Garca, A. E.; Pohorille, A.; Pratt, L. R. An information theory model of hydrophobic interactions. *Proc. Natl. Acad. Sci.* **1996**, *93*, 8951–8955.

(29) Sarupria, S.; Garde, S. Quantifying Water Density Fluctuations and Compressibility of Hydration Shells of Hydrophobic Solutes and Proteins. *Phys. Rev. Lett.* **2009**, *103*, 037803.

(30) Acharya, H.; Vembanur, S.; Jamadagni, S. N.; Garde, S. Mapping hydrophobicity at the nanoscale: Applications to heterogeneous surfaces and proteins. *Faraday Discuss.* **2010**, *146*, 353–365.

(31) Hess, B.; van der Vegt, N. F. A. Hydration thermodynamic properties of amino acid analogues: A systematic comparison of biomolecular force fields and water models. *J. Phys. Chem. B* **2006**, *110*, 17616–17626.

(32) Tilton, R. F., Jr.; Dewan, J. C.; Petsko, G. A. Effects of Temperature on Protein Structure and Dynamics: X-ray Crystallographic Studies of the Protein Ribonuclease-A at Nine Different Temperatures from 98 to 320 K. *Biochemistry* **1992**, *31*, 2469–2481.

(33) Zhou, Y.; Vitkup, D.; Karplus, M. Native Proteins are Surface-molten Solids: Application of the Lindemann Criterion for the Solid versus Liquid State. *J. Mol. Biol.* **1999**, *285*, 1371–1375.

(34) Vitkup, D.; Ringe, D.; Petsko, G. A.; Karplus, M. Solvent mobility and the protein 'glass' transition. *Nature* **2000**, *7*, 34–38.

(35) Kumar, P.; Yan, Z.; Xu, L.; Mazza, M. G.; Buldyrev, S. V.; Chen, S.; Sastry, S.; Stanley, H. E. Glass Transition in Biomolecules and the Liquid-Liquid Critical Point of Water. *Phys. Rev. Lett.* **2006**, *97*, 177802.

(36) Ringe, D.; Petsko, G. The glass transition in protein dynamics: what it is, why it occurs, and how to exploit it. *Biophys. Chem.* **2003**, *105*, 667–680.

(37) Leach, A. R. *Molecular Modelling: Principles and Applications*; Addison Wesley Longman Limited: China, 1998.

(38) Xantheas, S. S. Cooperativity and hydrogen bonding network in water clusters. *Chem. Phys.* **2000**, *258*, 225–231.

(39) Goldman, N.; Leforestier, C.; Saykally, R. J. A 'first principles' potential energy surface for liquid water from VRT spectroscopy. *Philos. Trans. R. Soc., London A* **2005**, *363*, 493–508.

(40) Vega, C.; Abascal, J. L. F.; Conde, M.; Aragones, J. What ice can teach us about water interactions:a critical comparison of the performance of different water models. *Faraday Discuss.* **2009**, *141*, 251–276.

(41) Vega, C.; Abascal, J. L. F. Relation between the melting temperature and the temperature of maximum density for the most common models of water. *J. Chem. Phys.* **2005**, *123*, 144504.

(42) Agarwal, M.; Alam, M. P.; Chakravarty, C. Thermodynamic, Diffusional and Structural Anomalies in Rigid-body Water Models *J. Phys. Chem. B* **2011**, *115*, 6935–6945.

(43) Scala, A.; Starr, F.; Nave, E.; Sciortino, F.; Stanley, H. Configurational entropy and diffusivity of supercooled water. *Nature* **2000**, *406*, 166–169.

(44) Jorgensen, W. L.; Chandrashekhar, J.; Madura, J.; Impey, R.; Klein, M. Comparison of simple potential functions for simulating liquid water. *J. Chem. Phys.* **1983**, *79*, 926–935.

(45) Neria, E.; Fischer, S.; Karplus, M. Simulation of activation free energies in molecular systems. *J. Chem. Phys.* **1996**, *105*, 1902–1921.

(46) Abascal, J. L. F.; Vega, C. A general purpose model for the condensed phases of water: TIP4P/2005. *J. Chem. Phys.* **2005**, *123*, 234505.

(47) Pi, H. L.; Aragones, J. L.; Vega, C; Noya, E. G.; Abascal, J. L. F.; Gonzalez, M. A.; McBride, C. Anomalies in water as obtained from computer simulations of the TIP4P/2005 model: density maxima, and density, isothermal compressibility and heat capacity minima. *Mol. Phys.* **2009**, *107*, 365–374.

(48) Sanz, E.; Vega, C.; Abascal, J. L. F.; MacDowell, L. G. Phase diagram of water from computer simulation. *Phys. Rev. Lett.* **2004**, *92*, 255701.

(49) Glass, D. C.; Krishnan, M.; Nutt, D. R.; Smith, J. C. Temperature Dependence of Protein Dynamics Simulated with Three Different Water Models. *J. Chem. Theory Comput.* **2010**, *6*, 1390–1400.

(50) Nutt, D. R.; Smith, J. C. Molecular Dynamics Simulations of Proteins: Can the Explicit Water Model Be Varied? *J Chem. Theory Comput.* **2007**, *3*, 1550–1560.

(51) Agarwal, M.; Kushwaha, H. R.; Chakravarty, C. Local Order, Energy and Mobility of Water Molecules in the Hydration Shell of Small Peptides. *J. Phys. Chem. B* **2010**, *114*, 651–659.

(52) Chau, P.-L.; Hardwick, A. J. A new order parameter for tetrahedral configurations. *Mol. Phys.* **1998**, *93*, 511–518.

(53) Mudi, A.; Ramaswamy, R.; Chakravarty, C. Signatures of multiple time-scale behaviour in the power spectra of water. *Chem. Phys. Lett.* **2003**, *376*, 683–689.

(54) Mudi, A.; Chakravarty, C. Effect of ionic solutes on the hydrogen bond network dynamics of water: power spectral analysis of aqueous NaCl solutions. *J. Phys. Chem. B* **2006**, *110*, 8422–8431.

(55) Sasai, M.; Ohmine, I.; Ramaswamy, R. Long time fluctuation of liquid water - 1/f spectrum of energy fluctuation in hydrogen bond network rearrangement dynamics. *J. Chem. Phys.* **1992**, *96*, 3045–3053.

(56) Mudi, A.; Chakravarty, C. Multiple Time-Scale Behavior of the Hydrogen-Bond Network in Water. *J. Phys. Chem. B* **2004**, *108*, 19607–19613.

(57) Mudi, A.; Chakravarty, C. Multiple Time-Scale Behavior of the Hydrogen-Bond Network in Water. *J. Phys. Chem. B* **2006**, *110*, 4502.

(58) Handgraaf, J.-W.; Zerbetto, F. Molecular Dynamics Study of Onset of Water Gelation around the Collagen Triple Helix. *Proteins* **2006**, *64*, 711–718.

(59) Sinha, S. K.; Bandyopadhyay, S. Differential Flexibility of the Secondary Structures of Lysozyme and the Structure and Ordering of Surrounding Water Molecules. *J. Chem. Phys.* **2011**, *134*, 115101.

(60) Mark, P.; Nilsson, L. Structure and Dynamics of the TIP3P, SPC, and SPC/E Water Models at 298K. *J. Phys. Chem. A* **2001**, *105*, 9954–9960.

(61) Abascal, J. L. F.; Vega, C. Dipole-Quadrupole Force ratios determine the ability of potential models to describe the phase diagram of water. *Phys. Rev. Lett.* **2007**, *98*, 237801–237804.

(62) Rick, S. W. A reoptimization of the five-site water potential (TIP5P) for use with Ewald sums. *J. Chem. Phys.* **2004**, *120*, 6085–6093.

(63) Smith, W.; Yong, C. W.; Rodger, P. M. DLPOLY: Application to molecular simulation. *Mol. Simulat.* **2002**, *28*, 385–471.

(64) Smith, W.; Forester, T. R.; Todorov, I. T. *The DL_POLY_2 User Manual 2008 Version 2.19*; STFC Daresvury Laboratory: Daresbury, U.K., 2008.

(65) Smith, W.; Yong, C. W.; Rodger, P. M. *DL_POLY 2.19*; CSE Department, STFC Darebusry Laboratory: Daresbury, U.K., 2002.

(66) Phillips, J. C.; Braun, R.; Wang, W.; Gumbart, J.; Tajkhorshid, E.; Villa, E.; Chipot, C.; Skeel, R. D.; Kale, L.; Schulten, K. Scalable Molecular Dynamics with NAMD. *J. Comput. Chem.* **2005**, *26*, 1781–1802.

(67) Phillips, J. C.; Braun, R.; Wang, W.; Gumbart, J.; Tajkhorshid, E.; Villa, E.; Chipot, C.; Skeel, R. D.; Kale, L.; Schulten, K. *NAMD 2.7*; University of Illinois: Urbana-Champaign, IL, 2005.

(68) Mahoney, M. W.; Jorgensen, W. L. A five-site model for liquid water and the reproduction of the density anomaly by rigid, nonpolarizable potential functions. *J. Chem. Phys.* **2000**, *112*, 8910–8922.

(69) Bolhuis, P. G. Transition-path sampling of β-hairpin folding. *Proc. Natl. Acad. Sci.* **2003**, *100*, 12129–12134.

(70) Humphrey, W.; Dalke, A.; Schulten, K. VMD: Visual Molecular Dynamics. *J. Mol. Graphics* **1996**, *14*, 33–38.

(71) Humphrey, W.; Dalke, A.; Schulten, K. *VMD: Visual Molecular Dynamics 1.8.7*; University of Illinois: Urbana-Champaign, IL, 1996.

(72) Jhon, Y. I.; No, K. T.; Jhon, M. S. Common features of orientational order at the temperature of maximum density for various water models: molecular dynamics study. *J. Phys. Chem. B* **2007**, *111*, 9897–9899.

(73) Jhon, Y. I.; No, K. T.; Jhon, M. S. The molecular-level relationship between the properties of liquid water molecules and orientational order. *Fluid Phase Equilib.* **2006**, *244*, 160–166.

(74) Sharma, R.; Mudi, A.; Chakravarty, C. Diffusional anomaly and network dynamics in liquid silica. *J. Chem. Phys.* **2006**, *125*, 044705.

(75) Sharma, R.; Mudi, A.; Chakravarty, C. Diffusional anomaly and network dynamics in liquid silica. *J. Chem. Phys.* **2009**, *130*, 199903.

(76) Jana, B.; Bagchi, B. Intermittent Dynamics, Stochastic Resonance and Dynamical Heterogeneity in Supercooled Liquid Water *J. Phys. Chem. B* **2009**, *113*, 2221–2224.

(77) Bosio, L.; Chen, S.-H.; Teixeira, J. Isochoric temperature differential of the X-ray structure factor and structural rearrangements in low-temprature heavy water. *Phys. Rev. A* **1983**, *27*, 1468–1475.

(78) Soper, A. K.; Philips, M. G. A new determination of the structure of water at 25°C. *Chem. Phys.* **1986**, *107*, 47–60.

(79) Kumar, P.; Buldyrev, S. V.; Stanley, H. E. A tetrahedral entropy for water. *Proc. Natl. Acad. Sci.* **2009**, *106*, 22130–22134.

(80) Bandyopadhyay, S.; Chakraborty, S.; Bagchi, B. Coupling between hydration layer dynamics and unfolding kinetics of HP-36 *J. Chem. Phys.* **2006**, *125*, 084912.

(81) Lee, S. L.; Debenedetti, P. G.; Errington, J. R. A computational study of hydration, solution structure, and dynamics in dilute carbohydrate solutions. *J. Chem. Phys.* **2005**, *122*, 204511.

(82) Mudi, A.; Chakravarty, C.; Ramaswamy, R. Spectral signatures of the diffusional anomaly in water. *J. Chem. Phys.* **2005**, *122*, 104507. **2006**, *124*, 069902.

(83) Sedlmeier, F.; Horinek, D.; Netz, R. R. Spatial Correlations of Density and Structural Fluctuations in Liquid Water: A Comparative Simulation Study. *J. Am. Chem. Soc.* **2011**, *133*, 1391–1398.

(84) Molinero, V.; Moore, E. B. Water Modeled as an Intermediate Element between Carbon and Silicon. *J. Phys. Chem. B* **2009**, *113*, 4008–4016.

(85) Te, J. A.; Tan, M.-L.; Ichiye, T. Solvation of glucose, trehalose, and sucrose by the soft-sticky dipole-quadrupole-octupole water model. *Chem. Phys. Lett.* **2010**, *491*, 218–223.

(86) Chaimovich, A.; Shell, M. S. Anomalous waterlike behavior in spherically-symmetric water models optimized with the relative entropy. *Phys. Chem. Chem. Phys.* **2009**, *11*, 1901–1915.

(87) Frenkel, D.; Smit, B. *Understanding Molecular Simulations: From Algorithms to Applications*; Academic Press: Waltham, MA, 2002.

(88) Allen, M.; Tildelsley, D. *Computer Simulation of Liquids*; Oxford University Press: New York, 1992.